Theoretical Studies on the Water-Assisted Hydrolysis of *N*,*N*-Dimethyl-*N*′-(2′,3′-dideoxy-3′-thiacytidine) Formamidine with Three Water Molecules

Jie Ying Gao,[†] Yi Zeng,[†] Cheng Hua Zhang,[†] and Ying Xue*[,†,‡]

College of Chemistry, Key Laboratory of Green Chemistry and Technology in Ministry of Education, Sichuan University, Chengdu 610064, People's Republic of China, and State Key Laboratory of Biotherapy, Sichuan University, Chengdu 610041, People's Republic of China

Received: August 5, 2008; Revised Manuscript Received: November 8, 2008

The water-assisted hydrolysis mechanism of *N*,*N*-dimethyl-*N*′-(2′,3′-dideoxy-3′-thiacytidine) formamidine (MFA-3TC) with three water molecules was studied by use of computational techniques. Optimized structures for all of the stationary points in the gas phase were investigated using the B3LYP/6-31+G(d,p) method. Single-point energies were determined employing the ab initio MP2 method in conjunction with the 6-311++G(d,p) basis set. Two possible pathways in the title reaction are considered, involving the attack of water molecule at first to the $C_{(1)}=N_{(1)}$ double bond (path A) and the attack of water molecule at first to the $C_{(1)}-N_{(2)}$ single bond (path B), respectively. A local microhydration model concerning three water molecules is adopted to mimic the system for the two reaction mechanisms above, where one water molecule is the nucleophilic reactant and the others are the auxiliary molecules. The calculated results indicate that the first steps in both pathways are the rate-limiting processes, and path A is more favorable than path B in the gas phase. In addition, bulk solvent effect is tested at the geometry optimization level by means of the conductor-like polarized continuum model (CPCM). Single-point computation was done at the MP2/6-311++G(d,p) level based on the geometries in the solution phase. Our results exhibit that the rate-limiting process in both pathways in water is the first step reaction, and path A is still favored. Two pathways are stepwise and slightly endothermic processes.

1. Introduction

Amidines are stable organic compounds with an >N−C=N− framework and should be good proton acceptors due to the unsaturated nitrogen atom. In recent years, amidines have been widely studied in proton affinities,[1] proton transfer,[2] tautomerization,[3–5] and thermal unimolecular decomposition process.[6,7] In addition, amidines have been investigated for their capacity to protect deoxyadenosine, deoxycytidine, 5-methyldeoxycytidine, cytidine, and deoxyguanosine since 1986.[8] Recently, as a precursor to the investigation of the deamination of the DNA base cytosine,[9] the hydrolysis mechanism of the simplest amidine compound, formamidine, has been investigated by Flinn and his co-workers.[10] They investigated the deamination of the simple formamidine with OH^-, H_2O, and H_3O^+ using HF, MP2, QCISD, and DFT/B3LYP, even up to G1 and G2 methods. In their work, for deamination with H_2O, two pathways were explored: the formation of a tetrahedral intermediate by the nucleophilic attack of water molecule to *C*=N double bond followed by a 1,3-proton shift to yield a product, and the formation of a tautomer of formamide by the nucleophilic attack of water molecule to C−N single bond followed by a 1,3-proton shift to dissociate to a product.

2′,3′-Dideoxy-3′-thiacytidine (3TC) is a modified nucleoside with cytosine as base, which has been known to have a good antiviral activity (HIV, HBV). Recently, Anastasi's group[11] has synthesized the potent nonclassical nucleoside antiviral drugs: formamidine-3TC analogues based on the *N*,*N*-diarylformamidine concept. In those new compounds, a dimethyl- or diarylamidine group was introduced by the replacing of formamidine side chains at the 4-N position of cytosine base. Those compounds not only enhanced the lipophilicity and bioavailability of the parent drug 3TC, but also served as the protector of the amino group in the base. The antiviral activity was exhibited only when the amidine side chains were hydrolyzed step by step to the corresponding free amino group (Scheme 1). In their experiment, the stability of this hydrolytic process, where the formamidine-3TC analogues were decomposed into the parent drug 3TC, was studied. It was found that the half-life of the enzyme-catalyzed hydrolysis for the title compound was observed to be in the range of 2−4.5 h in various biological media. Anastasi et al. inferred that the possible hydrolytic mechanism involves the formation of a common formamide-3TC intermediate as the first process (process 1) and then further hydrolysis of the intermediate (process 2).[11,12]

SCHEME 1: Schematic Pathway To Generate 3TC

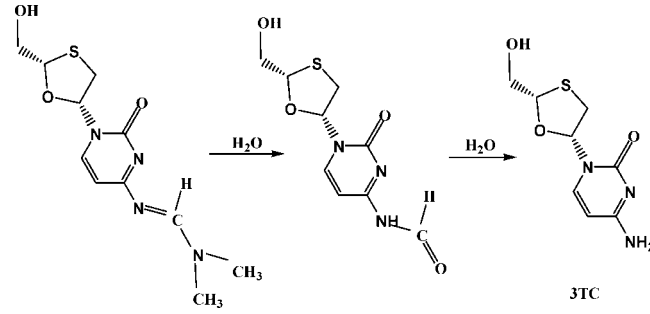

This new discovery inspired our group's great interests in investigating the hydrolysis mechanism of formamidine-3TC

* Corresponding author. Phone: +86 28 85418330. E-mail: yxue@scu.edu.cn.
† College of Chemistry, Sichuan University.
‡ State Key Laboratory of Biotherapy, Sichuan University.

10.1021/jp8069817 CCC: $40.75
Published on Web 12/05/2008

with dimethyl-group substitution (MFA-3TC) first at the theoretical level. In 2007, Wu et al.[13] examined the direct and water-assisted hydrolysis mechanisms of process 2 at the B3LYP/6-31G(d,p) and MP2/6-31G(d,p) levels of theory as well as by the Monte Carlo (MC) simulation and free energy perturbation methods. For the sake of simplicity and efficiency, they selected a simplified model to mimic the formamide-3TC through the replacement of the sugar ring of the cytidine nucleoside by an H atom. It was established that a water-assisted stepwise reaction path was the most favorable in six investigated pathways. More recently, Wu and co-workers[14] have investigated process 1, the hydrolysis mechanism of MFA-3TC to the formamide-3TC intermediate, based on a simplified model at the hybrid density functional theory B3LYP/6-31+G(d,p) method. In their work, Wu et al. not only investigated the direct reaction with one water molecule but also water-assisted hydrolysis mechanism with two or three water molecules in some appropriate steps. Additionally, the cluster-continuum model with six water molecules forming two solvation layers was utilized to evaluate the solvent effects on some steps, drawing a significant conclusion that the free energies of solvation changed slightly after the inclusion of the second solvation shell in the local microhydration surrounding. However, because they paid more attention to the influence of the second water shell to the energy barrier, the consecutive potential energy profile concerning the two reaction steps (the first is the nucleophilic attack of water, and the second is the proton transfer) has not been obtained. On the other hand, it is well-known that a study with the sugar ring group attached to the pyridine ring is more close to the real system. Zhang et al.[15] studied its hydrolysis mechanism with one water molecule using the density functional theory B3LYP/6-31+G(d,p) method. Similar to the results reported by Flinn et al.,[10] two pathways were explored. One was that the water molecule at first attacked the *C*═N double bond and a tetrahedral intermediate was generated. The other was that the water molecule at first attacked the C−N single bond and produced a tautomer of formamide. In that work, however, those transition states in each pathway were all four-membered cycle structures, where much of the ring constraint existed from the geometric view. The calculations exhibited that the activation energy barriers in the rate-controlling step were 42.3 and 56.0 kcal/mol in the gas phase for path A and for path B, respectively. Even though the energies decreased in water (being 39.6 kcal/mol for path A and 49.2 kcal/mol for path B, respectively), we still thought the results were not more favorable due to the high energy barriers.

In this present study, our motif is to clearly clarify the detailed consecutive water-assisted mechanism of MFA-3TC, and to shed great light on the question whether the water-assisted hydrolysis contributes to the lowering of the high energy barriers of the direct mechanism or not, which is a continuous work of Zhang et al.[15] Taking the major effect of the inner layer into account,[14] we describe the mechanism with three water molecules around the reaction centers for a local microhydration surrounding. Among the three water molecules, one is the nucleophilic reactant, another serves as a bridge to help the transfer of the hydrogen atom, and the third one makes the cooperation effect to stabilize the structure through forming the hydrogen bond. For the title reaction, similar to the work of Zhang et al.,[15] two possible pathways were assumed here, as shown in Scheme 2. For the gas-phase reactions, optimized structures for all of the stationary points were determined at the density functional theory (B3LYP) method with the 6-31+G(d,p) basis set. Single-point MP2 calculations (MP2/6-311++G(d,p)//B3LYP/6-31+G(d,p)) were carried out to obtain more credible energy

SCHEME 2: Possible Water-Assisted Hydrolysis Pathways of MFA-3TC

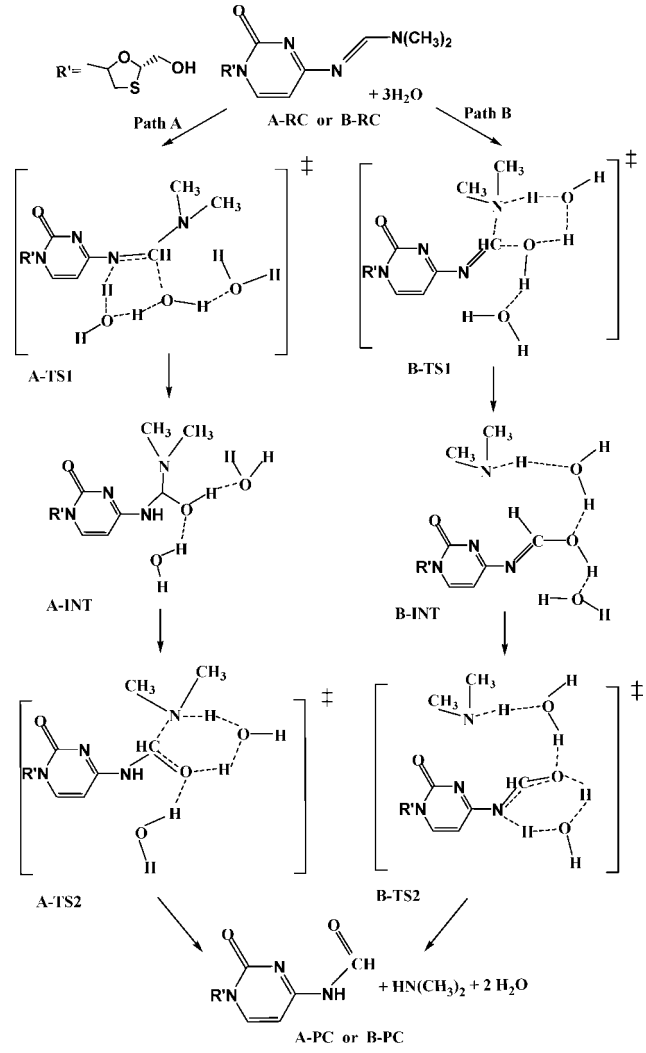

information. In addition, the natural bond orbital (NBO) analysis was also carried out to observe the bond order changes in the process of the reaction, and the solvent effect was examined by using the conductor-like polarizable continuum model (CPCM). The investigation for the title reaction may provide very useful information for studying the enzyme-catalyzed hydrolysis reaction in human body and controlling the release of drug.

2. Computational Details

In this study, the geometric structures of all of the reactant complexes (RC), transition states (TS), intermediates (INT), and product complexes(PC) in two pathways of the hydrolysis reaction of MFA-3TC with three water molecules in the gas phase were optimized at the density functional theory B3LYP/6-31+G(d,p) level. The nature of the stationary points was confirmed by the harmonic frequency analysis as a minimum with all positive frequencies or as a transition state with only one imaginary frequency. Next, the intrinsic reaction coordinate (IRC)[16–18] calculations were performed to verify the transition state associated with the correct reactant and product. The thermodynamic data such as the zero point vibrational energy correction, enthalpy, and Gibbs free energy at the temperature of 298.15 K and the pressure of 1.0 atm were obtained via the harmonic frequency calculation at the B3LYP/6-31+G(d,p)

SCHEME 3: Atomic Numbering of the Reaction System in the Water-Assisted Hydrolysis of MFA-3TC

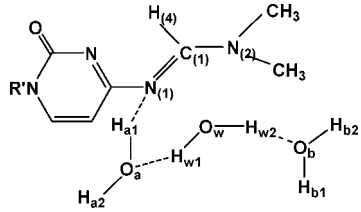

level. To obtain more credible energy information, single-point MP2 calculations, MP2/6-311++G(d,p)//B3LYP/6-31+G(d,p), were carried out. The natural charges and Wiberg bond orders were calculated for all optimized structures using Natural Bond Orbital Theory (NBO)[19] at the B3LYP/6-31+G(d,p) level. The atomic numbering of the system involved in the center of the hydrolysis is given in Scheme 3. In the following, the reported energy barriers were calculated by comparing the energies of the transition states with those of the corresponding intermediates.

In addition, the cluster-continuum model was employed to estimate solvation energies in aqueous solution ($\varepsilon = 78.39$). In our model, three water molecules around the reaction centers were included to simulate a local microhydration surrounding, where one water molecule is the nucleophilic reactant and the others are the auxiliary molecules (see Scheme 3). This hybrid cluster-continuum solvation model has been utilized in a number of systems.[14,20–23] To examine the solvent effects accurately, we adopted the B3LYP/6-31+G(d,p) level in collaboration with the conductor-like polarized continuum model (CPCM)[24] to further optimize the geometries of the stationary points in water. Furthermore, single-point calculations were performed at the MP2/6-311++G(d,p) level based on the optimized geometries in the solution phase. All calculations mentioned above were performed with the Gaussian 03 program.[25]

3. Results and Discussion

3.1. Optimized Structures in the Gas Phase. The water-assisted hydrolysis mechanism of MFA-3TC with two pathways is clarified in this work (Scheme 2). In path A, a tetrahedral intermediate is generated by the addition of H_2O to the $C_{(1)}=N_{(1)}$ double bond in the amidine group in the first step, and then the proton transfer to the $N_{(2)}$ atom of the amino group. In path B, the nucleophilic attack of H_2O at the $C_{(1)}$ atom and the simultaneous proton transfer to the $N_{(2)}$ atom of amino group lead to the cleavage of the $C_{(1)}-N_{(2)}$ single bond in the amidine group. Sequentially, the corresponding product is offered by the proton shift to the $N_{(1)}$ atom. As for the two additional water molecules in the two pathways, one water molecule serves as a bridge to help the transfer of the hydrogen atom, and the other one makes the cooperation effect to stabilize the structure through forming the hydrogen bond in another side. The two pathways, paths A and B, are the stepwise processes.

3.1.1. Path A. The optimized geometries and important bond lengths for the stationary points are shown in Figure 1. As described in Figure 1, the reactant complex A-RC is generated due mainly to the H-bond network, where three water molecules are connected with two hydrogen bonds. A-TS1 is a six-membered ring transition state. From A-RC to A-TS1, one can see that the $C_{(1)}-O_w$ bond is partially produced at first. The analysis of the vibrational mode indicates that this step is associated with the coupling of the transfer of H_{a1} atom from O_a to $N_{(1)}$ atom and the transfer of H_{w1} atom from O_w to O_a atom. After surmounting the transition state A-TS1, the intermediate A-INT is formed. A-INT is a tetrahedral geometry similar to the hydrolysis mechanism with one water molecule.[15] Although the distance of $H_{b1}-N_{(2)}$ is 1.9030 Å in A-INT, it also indicates that the H_{b1} atom can be transferred from O_b to $N_{(2)}$ atom due to the short distance. For the geometry of A-INT, the distance of $C_{(1)}-N_{(1)}$ is 1.4555 Å, longer than those in A-RC and A-TS1 by 0.1345 and 0.0429 Å, respectively. This indicates that the $C_{(1)}-N_{(1)}$ bond of A-INT becomes weaker and changes from the double bond to the single bond. In the next step, the transition state A-TS2, still a six-membered transition state, was located in our calculations. From A-INT to A-TS2, the proton transfer toward the $N_{(2)}$ leads to an elongation of 0.0845 Å for $C_{(1)}-N_{(2)}$ bond length and a reduction of 0.0458 Å for $C_{(1)}-O_w$ bond in contrast to those of the A-INT. The imaginary frequency is 936.13i cm^{-1}, which is associated with the coupling of the transfer of H_{b1} atom from O_b to $N_{(2)}$ atom and the transfer of H_{w2} atom from O_w to O_b atom. After the transition state A-TS2 is overcome, the product A-PC is produced. In A-PC, the $N_{(2)}-C_{(1)}$ distance is 2.9659 Å, which indicates that this bond has already been broken. The $C_{(1)}-O_w$ bond length is 1.2357 Å. It is shortened by 0.1352 Å as compared to that of the A-TS2, implying that the bond $C_{(1)}-O_w$ changes from the single bond to the double bond.

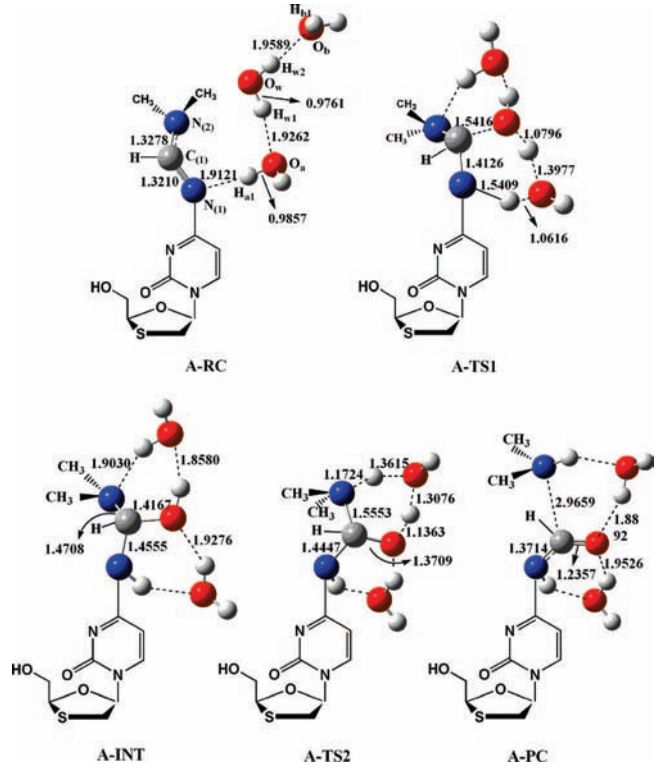

Figure 1. The optimized structures of the stationary points in path A obtained by the B3LYP/6-31+G(d,p) method (bond length in angstroms).

3.1.2. Path B. The optimized geometries and important bond lengths for the stationary points are depicted in Figures 2 and 3. For the reactant complex B-RC, the H_{w2}, H_{b1}, and H_{a1} atoms interact, respectively, with the O_b, O_a, and $N_{(1)}$ atoms to form three hydrogen bonds. We located the transition state B-TS0 in our calculation. Its structure is shown in Figure 3. In B-TS0, the imaginary frequency is 134.50i cm^{-1}, associated with the nucleophilic attack of the O_w atom to the $C_{(1)}$ atom. In the forward reaction direction, the intermediate B-INT0 was also located (see Figure 3). Yet the Gibbs free energy (G) of B-INT0 is 0.0458 kcal/mol higher than that of B-TS0 at the B3LYP/6-

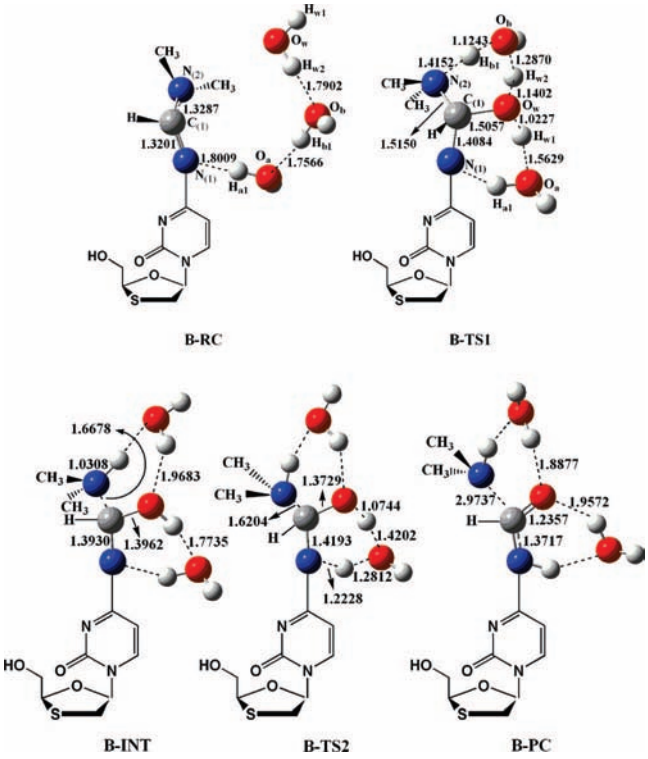

Figure 2. The optimized structures of the stationary points in path B obtained by the B3LYP/6-31+G(d,p) method (bond length in angstroms).

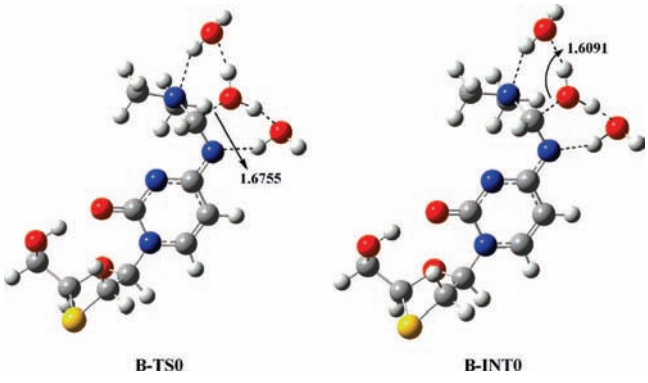

Figure 3. The optimized structures of the stationary points in path B obtained by the B3LYP/6-31+G(d,p) method (bond length in angstroms).

31+G(d,p) level, indicating that the transition state B-TS0 can not stably exist. On the other hand, from the molecular geometries displayed in Figures 2 and 3, one can see that the optimized structure of the next transition state B-TS1 is very close to those of B-TS0 and B-INT0. Accordingly, in the following section, the process we reported is directly from reactant complex B-RC to the transition state B-TS1. B-TS1 is a six-membered cycle transition state, which is directly associated with the $C_{(1)}-N_{(2)}$ bond cleavage, the formation of $C_{(1)}-O_w$ bond, and the proton transfer to $N_{(2)}$ atom. The single bond $C_{(1)}-N_{(2)}$ is elongated by 0.1863 Å as compared to that in B-RC. The bond $O_w-C_{(1)}$ distance is 1.5057 Å, which indicates that the $C_{(1)}-O_w$ bond is almost formed at first. The analysis of the imaginary frequency vibration mode reveals that this step is associated with the coupling of the transfer of H_{b1} atom from O_b to $N_{(2)}$ atom and the transfer of H_{w2} atom from O_w to O_b atom. In the intermediate B-INT, the $C_{(1)}-N_{(2)}$ bond length is 1.6678 Å. It is implying that the amine compound has been formed. When proceeding from B-INT to B-TS2, similar to the mechanism of path A, a six-membered ring transition state is also shaped. Because of the proton transfer, the $C_{(1)}-N_{(1)}$ bond distance is elongated by 0.0263 Å and the $C_{(1)}-O_w$ bond length is shortened by 0.0233 Å as compared to that of the B-INT. The imaginary frequency is 1019.42i cm^{-1}, which is associated with the coupling of the transfer of H_{a1} atom from O_a to $N_{(1)}$ atom and the transfer of H_{w1} atom from O_w to O_a atom. The final product complex B-PC is obtained after surmounting the transition state B-TS2. For B-PC, the bond $C_{(1)}-O_w$ has changed from the single bond to the double bond. As compared to B-INT, the $C_{(1)}-N_{(1)}$ bond length is shortened to 1.3717 Å by a reduction of 0.0213 Å, which is mainly due to the $p-\pi$ conjugative effect among the new-formed acyl group and the pyramiding ring in the B-PC.

3.2. Energetics in the Gas Phase. ***3.2.1. Path A.*** The changes in electronic energies (ΔE) and Gibbs free energies (ΔG) are given in Table 1. The calculated total relative energy profiles are presented in Figure 4. As depicted in Figure 4, for the first step, the energy barrier is 34.01 kcal/mol at the B3LYP/6-31+G(d,p) level in the gas phase, while it decreases to 29.70 kcal/mol at the MP2/6-311++G(d,p)//B3LYP/6-31+G(d,p) level. For the second step, the energy barriers are 12.29 kcal/mol at the B3LYP/6-31+G(d,p) level and 14.26 kcal/mol at the MP2/6-311++G(d,p)//B3LYP/6-31+G(d,p) level, respectively. Our calculations figure out that the relative energy of A-TS1 is higher than that of A-TS2 at both levels (the B3LYP/6-31+G(d,p) and the MP2/6-311++G(d,p)//B3LYP/6-31+G(d,p)), which indicates the rate-limiting process of path A in the gas phase is the first step reaction. From Figure 4 and Table 1, it can be seen that the energy increases by 3.18 kcal/mol from reactant to product at the MP2/6-311++G(d,p)//B3LYP/6-31+G(d,p) level, which implies that the process is slightly endothermic.

3.2.2. Path B. The changes in electronic energies (ΔE) and Gibbs free energies (ΔG) are also given in Table 1. The calculated total relative energy profiles are presented in Figure 4. As described in Figure 4, for the first step, the energy barrier is 42.58 kcal/mol at the B3LYP/6-31+G(d,p) level in the gas phase, while it diminishes to 37.29 kcal/mol at the MP2/6-311++G(d,p)//B3LYP/6-31+G(d,p) level. For the second step, the energy barriers are 5.67 kcal/mol at the B3LYP/6-31+G(d,p) level and 7.68 kcal/mol at the MP2/6-311++G(d,p)//B3LYP/6-31+G(d,p) level, respectively. Our calculations determine that the relative energy of B-TS1 is higher than that in the corresponding second transition state B-TS2 at both levels, which indicates the rate-limiting process of path B in the gas phase is the first step reaction. As shown in Figure 4, one can see that this pathway is also endothermic. From Table 1, the energy barrier in the rate-controlling step of path A (29.70 kcal/mol) is significantly lower than that of path B (37.29 kcal/mol) at the MP2/6-311++G(d,p)//B3LYP/6-31+G(d,p) level. Herein, the water-assisted hydrolysis mechanism of MFA-3TC in the gas phase may be more favorable for path A than for path B. Considering the contributions of entropy, the Gibbs free energies at the B3LYP/6-31+G(d,p) level of both pathways were also discussed, indicating that path A (40.53 kcal/mol) is still more favorable than path B (45.21 kcal/mol).

The changes in electronic energies (ΔE) and Gibbs free energies (ΔG) of the direct hydrolysis reaction at the B3LYP/6-31+G(d,p) level in the gas phase, which were reported in the previous work,[15] are also depicted in Table 1. According to the energy data in Table 1, as expected, the energy barriers of both water-assisted pathways decrease dramatically in com-

TABLE 1: Changes of Electronic Energies and Gibbs Free Energies for Two Pathways in the Gas Phase and in Water (in kcal/mol)

	B3LYP/6-31+G(d,p)					MP2/6-311++G(d,p)//B3LYP/6-31+G(d,p)	
	ΔE (gas)[a]	ΔG (gas)[a]	ΔE (gas)	ΔG (gas)	ΔE (sol)	ΔE (gas)	ΔE (sol)
Path A							
RC→TS1	42.33	42.42	34.01	40.53	39.00	29.70	32.19
RC→INT	6.88	11.53	1.90	9.62	7.60	−3.34	2.39
INT→TS2	28.79	26.63	12.29	10.78	11.68	14.26	11.71
INT→PC	−2.13	−7.85	−1.88	−8.23	−5.19	6.53	5.27
RC→PC	4.75	3.68	0.02	1.39	2.41	3.18	7.66
Path B							
RC→TS1	55.95	56.21	42.58	45.21	41.54	37.29	35.55
RC→INT	17.55	16.32	20.13	24.99	17.31	14.29	10.02
INT→TS2	30.97	28.76	5.67	3.06	5.43	7.68	8.00
INT→PC	−10.47	−10.04	−14.28	−21.61	−13.65	−5.73	0.06
RC→PC	7.08	6.28	5.85	3.39	3.66	8.56	10.08

[a] The changes in electronic energies and Gibbs free energies in the direct hydrolysis reactions (ref 15).

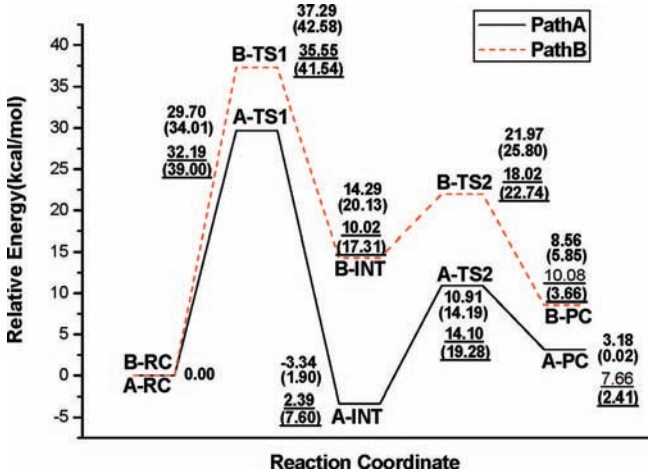

Figure 4. Potential energy profiles along two pathways (top values, ΔE at the MP2/6-311++G (d,p)//B3LYP/6-31+G(d,p) level in the gas phase; values in parentheses, ΔE at the B3LYP/6-31+G(d,p) level in the gas phase; underlined values, ΔE at the CPCM/MP2/6-311++G(d,p)// B3LYP/6-31+G(d,p) level in water; underlined values with brackets, ΔE at the CPCM/B3LYP/6-31+G(d,p) level) in water.

parison with those of the direct hydrolysis[15] due to the contribution of the auxiliary water molecules. For path A, the energy barriers of the direct and the water-assisted hydrolysis reactions are 42.33 and 34.01 kcal/mol, respectively. For path B, the energy barrier of the water-assisted hydrolysis is ca. 15 kcal/mol lower than that in the direct hydrolysis reaction. The calculations exhibit that the formation of the favored six-membered ring structure in the transition state leads to the reduction of the ring constraint for the proton transfer, and most of the energy saving has been achieved for its small deformation.

3.3. Solvent Effects of Bulk Water on the Hydrolysis of MFA-3TC. In view of the fact that the hydrolysis of MFA-3TC actually takes place in the human body solution, it is of great significance to study the influence of solvent water on the reaction. To estimate this solvent effect in water, the geometric structures of all stationary points along two pathways were reoptimized at the B3LYP/6-31+G(d,p) level with the CPCM model. Cartesian coordinates optimized in water are given in the Supporting Information. The important bond lengths of the transition states of the two pathways in the gas phase and water are listed in Tables 2 and 3 for comparison, implying that the small geometrical changes are induced by the presence of the bulk water.

TABLE 2: Selected Geometrical Parameters for the Transition States Optimized at the B3LYP/6-31+G(d,p) level in the Gas Phase and in Water[a]

		TS1		TS2	
	bond length	gas	water	gas	water
path A	$C_{(1)}-O_w$	1.5416	1.5070	1.3709	1.3819
	$C_{(1)}=N_{(1)}$	1.4126	1.4264	1.4447	1.4361
	$N_{(1)}-H_{a1}$	1.5409	1.5753	1.0204	1.0221
	$H_{a1}-O_a$	1.0616	1.0543	1.9895	2.0212
	$H_{w1}-O_a$	1.3977	1.2688	0.9835	0.9773
	$H_{w1}-O_w$	1.0796	1.1622	1.8200	1.9716
	$C_{(1)}-N_{(2)}$	1.4655	1.4631	1.5553	1.5495
	$N_{(2)}-H_{b1}$	1.8413	2.0064	1.1724	1.1439
	$H_{b1}-O_b$	0.9977	0.9854	1.3615	1.4297
	$H_{w2}-O_b$	1.6105	1.6249	1.3076	1.3924
	$H_{w2}-O_w$	1.0101	1.0103	1.1363	1.0909
path B	$C_{(1)}-O_w$	1.5057	1.5031	1.3729	1.3804
	$C_{(1)}=N_{(1)}$	1.4084	1.4103	1.4193	1.4297
	$N_{(1)}-H_{a1}$	1.6850	1.8629	1.2228	1.1932
	$H_{a1}-O_a$	1.0174	0.9942	1.2812	1.3252
	$H_{w1}-O_a$	1.5629	1.6881	1.4202	1.5461
	$H_{w1}-O_w$	1.0227	1.0046	1.0744	1.0349
	$C_{(1)}-N_{(2)}$	1.5150	1.4884	1.6204	1.5748
	$N_{(2)}-H_{b1}$	1.4152	1.6223	1.0338	1.0443
	$H_{b1}-O_b$	1.1243	1.0481	1.8746	1.7678
	$H_{w2}-O_b$	1.2870	1.1924	0.9791	0.9786
	$H_{w2}-O_w$	1.1402	1.2341	1.8995	3.5781

[a] Bond distances are in angstroms.

The changes in electronic energies (ΔE(sol)) of both pathways in water at the B3LYP/CPCM/6-31+G(d,p) level are summarized in Table 1. The single-point energies were calculated at the MP2/CPCM/6-311++G(d,p) level on the basis of the optimized geometries in water to assess the accuracy of the B3LYP energies. The corresponding energy changes along two pathways are also presented in Table 1. For path A, the energy barrier of the first step in water is 2.49 kcal/mol higher than that in the gas phase, attributed to that the dipole moment of A-TS1 (8.0770 debye) is less than that of A-RC (9.0744 debye), and the transition state A-TS1 is destabilized in solvent water by solvation. For path B, on the contrary, the dipole moment of B-TS1 (8.5109 debye) is larger than that of B-RC (7.0263 debye), and then the solvation of water on B-TS1 is stronger than that on B-RC. As a result, the solvent water stabilizes the transition state B-TS1, leading to a reduction of energy barrier by 1.74 kcal/mol as compared to that in the gas phase. From Table 1, it can be seen that, for path A and path B, the energy barrier of the first step process is significantly higher than that

TABLE 3: Percentage of Evolution of Bond Orders $(\%Ev)_i$ and Synchronicity (S_y)

	step 1				step 2			
		%Ev	S_y	S_y[a]		%Ev	S_y	S_y[b]
path A	$C_{(1)}-O_w$	79.59	0.715	0.835	O_b-H_{b1}	59.61	0.765	0.694
	$C_{(1)}-N_{(1)}$	72.63			$N_{(2)}-H_{b1}$	52.05		
	O_w-H_{w1}	36.97			O_w-H_{w2}	38.89		
	O_a-H_{w1}	28.94			O_b-H_{w2}	37.44		
	O_a-H_{a1}	25.68			$C_{(1)}-O_w$	15.47		
	$N_{(1)}-H_{a1}$	22.75			$C_{(1)}-N_{(2)}$	14.39		
path B	$C_{(1)}-O_w$	81.92	0.801	0.749	O_a-H_{a1}	52.59	0.733	0.966
	$C_{(1)}-N_{(2)}$	69.72			$N_{(1)}-H_{a1}$	52.50		
	O_w-H_{w2}	43.12			O_w-H_{w1}	25.10		
	$N_{(2)}-H_{b1}$	38.72			O_a-H_{w1}	24.51		
	O_b-H_{w2}	37.01			$C_{(1)}-O_w$	9.63		
	O_b-H_{b1}	33.15			$C_{(1)}-N_{(1)}$	0.00		

[a] The synchronicity values for step 1 of two pathways in the direct hydrolysis reactions (ref 15). [b] The synchronicity values for step 2 of two pathways in the direct hydrolysis reactions (ref 15).

in the corresponding second step. Accordingly, the first step is also a rate-limiting process in solution. The energy barriers of the rate-determining step for path A and path B are 32.19 and 35.55 kcal/mol, respectively. So path A is still more favorable for the title reaction in water.

3.4. Bond Order Analysis. To gain insight into the various bond-breaking or bond-making processes, the Wiberg bond order values were obtained through NBO analysis[19] at the B3LYP/6-31+G(d,p) level in the gas phase. The percentage of evolution of bond orders (%Ev) is given by

$$(\%\mathrm{Ev})_i = 100 \times [B_i^{\mathrm{TS}} - B_i^{\mathrm{RE}}]/[B_i^{\mathrm{PR}} - B_i^{\mathrm{RE}}] \quad (1)$$

where the superscripts TS, RE, and PR denote the transition state, reactant, and product, respectively. Another concept, synchronicity (S_y), proposed by Moyano et al.,[26] is usually used to represent the global nature of bond-breaking/-forming process in the reaction and expressed by

$$S_y = 1 - \frac{\sum_{i=1}^{n} \frac{(\%\mathrm{Ev})_i - (\%\mathrm{Ev})_{\mathrm{av}}}{(\%\mathrm{Ev})_{\mathrm{av}}}}{2n-2} \quad (2)$$

In eq 2, n refers to the number of bonds directly involved in the reaction, and here the average $(\%Ev)_{av}$ is

$$(\%\mathrm{Ev})_{\mathrm{av}} = \frac{1}{n}\sum_{i=1}^{n} (\%\mathrm{Ev})_i \quad (3)$$

Percentage of evolution of bond orders (%Ev) and synchronicity (S_y) are presented in Table 2. For step 1 of path A, the %Ev values of A-TS1 indicate that the $C_{(1)}-O_w$ bond-forming (%Ev = 79.59%) and the $C_{(1)}=N_{(1)}$ bond-changing from double bond to single bond (%Ev = 72.63%) are the most advanced among all of the processes, which corresponds to the nucleophilic attack of H_2O to the $C_{(1)}$ atom. The O_w-H_{w1} bond-breaking (%Ev = 36.97%), the O_a-H_{w1} bond-forming (%Ev = 28.94%), the O_a-H_{a1} bond-breaking (%Ev = 25.68%), and the $N_{(1)}-H_{a1}$ bond-forming (%Ev = 22.75%) are almost a simultaneous process. It shows that the proton transfers of H_{a1} from the O_a atom to the $N_{(1)}$ atom and H_{w1} from the O_w atom to the O_a atom are very late. For step 2 of path A, the O_b-H_{b1} bond-breaking and the $N_{(2)}-H_{b1}$ bond-making are very early with the %Ev values of 59.61% and 52.05%, respectively, which corresponds to the transfer of the H_{b1} atom from O_b to the $N_{(2)}$ atom. The O_w-H_{w2} bond-breaking and O_b-H_{w2} bond-making are almost a simultaneous process (with %Ev values of 38.89% and 37.44% for the O_w-H_{w2} and O_b-H_{w2} bonds, respectively), which corresponds to the transfer of the H_{w2} atom from the O_w atom to the O_b atom. The $C_{(1)}-O_w$ bond-changing from single bond to double bond (%Ev = 15.47%) and the cleavage of the $C_{(1)}-N_{(2)}$ bond (%Ev = 14.39%) hardly proceed. The synchronicity values of 0.715 and 0.765 for step 1 and step 2 in path A, respectively, show that the two steps of this mechanism are slightly asynchronous. The results are different from those in the direct hydrolysis mechanism, where the first step is synchronous ($S_y = 0.835$) and the second step is asynchronous ($S_y = 0.694$).[15]

For step 1 of path B, the %Ev values indicate that the $C_{(1)}-O_w$ bond-forming (%Ev = 81.92%) and the $C_{(1)}-N_{(2)}$ bond-breaking process (%Ev = 69.72%) is more advanced than the transfers of H_{b1} from the O_b atom to the $N_{(2)}$ atom in the $C_{(1)}-N_{(2)}$ bond and H_{w2} from the O_w atom to the O_b atom (with %Ev values of 43.12%, 38.72%, 37.01%, and 33.15% for the O_w-H_{w2}, $N_{(2)}-H_{b1}$, O_b-H_{w2}, and O_b-H_{b1} bonds, respectively). For step 2 of path B, the transfer of the H_{a1} atom from the O_a atom to the $N_{(1)}$ atom is most advanced (with %Ev values of 52.59% and 52.50% for the O_a-H_{a1} and $N_{(1)}-H_{a1}$ bonds, respectively). The O_w-H_{w1} bond-breaking and O_a-H_{w1} bond-making are almost a simultaneous process (with %Ev values of 25.10% and 24.51% for the O_w-H_{w1} and O_a-H_{w1} bonds, respectively), which corresponds to the transfer of the H_{w1} atom from the O_w atom to the O_a atom. The $C_{(1)}-O_w$ bond-changing from single bond to double bond (%Ev = 9.63%) and the $C_{(1)}=N_{(1)}$ bond-changing from double bond to single bond (%Ev = 0.00%) hardly proceed. The synchronicity value of 0.801 reveals that the first step can be viewed as a synchronous process. The second step in path B is a slightly asynchronous process with $S_y = 0.733$. The results are reverse from those in the direct hydrolysis, which is a slightly synchronous process for the first step ($S_y = 0.749$) and a very synchronous process for the second step ($S_y = 0.966$).[15]

4. Conclusion

In this study, the microhydration model for the water-assisted hydrolysis mechanism of MFA-3TC with three water molecules was studied with the B3LYP/6-31+G(d,p) and MP2/6-311++G(d,p)//B3LYP/6-31+G(d,p) methods. The solvent effect of water was evaluated by using the conductor-like polarizable continuum model (CPCM). Two possible water-assisted pathways were taken into account in our calculations. The results indicated that two pathways are stepwise and slightly endothermic processes. Both in the gas phase and in water, the rate-controlling step is the first one for those two mechanisms, and path A is the most favorable pathway of the reaction. As compared to the results of the direct hydrolysis,[15] the electronic energy barriers (ΔE) and Gibbs free energies (ΔG) in each step of both pathways decrease dramatically about 10−20 kcal/mol at the B3LYP/6-31+G(d,p) level. Such calculations may provide very useful information for studying this type of reaction.

Acknowledgment. This project has been supported by the National Natural Science Foundation of China (Grant Nos. 20473055, 20773089, and 20835003) and by the Scientific Research Foundation for the Returned Overseas Chinese Scholars, State Education Ministry (Grant No. 20071108-18-15).

Supporting Information Available: Optimized Cartesian coordinates and geometrical structures of all stationary points along the potential energy profile. This material is available free of charge via the Internet at http://pubs.acs.org.

References and Notes

(1) Peeters, D.; Leroy, G.; Wilante, C. *J. Mol. Struct.* **1997**, *416*, 21.
(2) Simperler, A.; Mikenda, W.; Schwarz, K. *Chem.-Eur. J.* **2001**, *7*, 1606.
(3) Zhang, Q.; Bell, R.; Truong, T. N. *J. Phys. Chem.* **1995**, *99*, 592.
(4) Nguyen, K. A.; Gordon, M. S.; Truhlar, D. G. *J. Am. Chem. Soc.* **1991**, *113*, 1596.
(5) Lim, J.-H.; Lee, E. K.; Kim, Y. *J. Phys. Chem.* **1997**, *101*, 2233.
(6) Andrés, J.; Beltran, A.; Carda, M.; Krechl, J.; Monterde, J.; Silla, E. *J. Mol. Struct. (THEOCHEM)* **1992**, *254*, 465.
(7) Almatarneh, M. A.; Flinn, C. G.; Poirier, R. A. *Can. J. Chem.* **2005**, *83*, 2082.
(8) McBride, L. J.; Kierzek, R.; Beaucage, S. L.; Caruthers, M. H. *J. Am. Chem. Soc.* **1986**, *108*, 2024.
(9) Almatarneh, M. A.; Flinn, C. G.; Poirier, R. A.; Sokalski, W. A. *J. Phys. Chem. A* **2006**, *110*, 8227.
(10) Flinn, C. G.; Poirier, R. A. *J. Phys. Chem. A* **2003**, *107*, 11174.
(11) Anastasi, C.; Hantz, O.; Clercq, F. D.; Pannecouque, C. *J. Med. Chem.* **2004**, *47*, 1183.
(12) Kalman, T. I.; Reddy, A. R. V. *Ann. N.Y. Acad. Sci.* **1990**, *616*, 540.
(13) Wu, Y.; Xue, Y.; Xie, D. Q.; Kim, C. K.; Yan, G. S. *J. Phys. Chem. B* **2007**, *111*, 2357.
(14) Wu, Y.; Jin, L.; Xue, Y.; Xie, D. Q.; Kim, C. K.; Guo, Y.; Yan, G. S. *J. Comput. Chem.* **2008**, *29*, 1222.
(15) Zhang, C.; Xue, Y. *Sci. China, Ser. B* **2008**, *51*, 911.
(16) Fukui, K. *J. Phys. Chem.* **1970**, *74*, 4161.
(17) Gonzalez, C.; Schlegel, H. B. *J. Chem. Phys.* **1989**, *90*, 2154.
(18) Gonzalez, C.; Schlegel, H. B. *J. Phys. Chem.* **1990**, *94*, 5523.
(19) Reed, A. E.; Curtiss, L. A.; Weinhold, F. *Chem. Rev.* **1988**, *88*, 899.
(20) Cao, Z. J.; Lin, M. H.; Zhang, Q. E.; Mo, Y. R. *J. Phys. Chem. A* **2004**, *108*, 4277.
(21) Xue, Y.; Kim, C. K.; Guo, Y.; Xie, D. Q.; Yan, G. S. *J. Comput. Chem.* **2005**, *26*, 994.
(22) Li, Q. G.; Xue, Y.; Yan, G. S. *J. Mol. Struct. (THEOCHEM)* **2008**, *868*, 55.
(23) Zeng, Y.; Xue, Y.; Yan, G. S. *J. Phys. Chem. B* **2008**, *112*, 10659.
(24) Barone, V.; Cossi, M. *J. Phys. Chem. A* **1998**, *102*, 1995.
(25) Frisch, M. J.; Trucks, G. W.; Schlegel, H. B.; Scuseria, G. E.; Robb, M. A.; Cheeseman, J. R.; Montgomery, J. A., Jr.; Vreven, T.; Kudin, K. N.; Burant, J. C.; Millam, J. M.; Iyengar, S. S.; Tomasi, J.; Barone, V.; Mennucci, B.; Cossi, M.; Scalmani, G.; Rega, N.; Petersson, G. A.; Nakatsuji, H.; Hada, M.; Ehara, M.; Toyota, K.; Fukuda, R.; Hasegawa, J.; Ishida, M.; Nakajima, T.; Honda, Y.; Kitao, O.; Nakai, H.; Klene, M.; Li, X.; Knox, J. E.; Hratchian, H. P.; Cross, J. B.; Bakken, V.; Adamo, C.; Jaramillo, J.; Gomperts, R.; Stratmann, R. E.; Yazyev, O.; Austin, A. J.; Cammi, R.; Pomelli, C.; Ochterski, J. W.; Ayala, P. Y.; Morokuma, K.; Voth, G. A.; Salvador, P.; Dannenberg, J. J.; Zakrzewski, V. G.; Dapprich, S.; Daniels, A. D.; Strain, M. C.; Farkas, O.; Malick, D. K.; Rabuck, A. D.; Raghavachari, K.; Foresman, J. B.; Ortiz, J. V.; Cui, Q.; Baboul, A. G.; Clifford, S.; Cioslowski, J.; Stefanov, B. B.; Liu, G.; Liashenko, A.; Piskorz, P.; Komaromi, I.; Martin, R. L.; Fox, D. J.; Keith, T.; AlLaham, M. A.; Peng, C. Y.; Nanayakkara, A.; Challacombe, M.; Gill, P. M. W.; Johnson, B.; Chen, W.; Wong, M. W.; Gonzalez, C.; Pople, J. A. *Gaussian 03. Version D01*; Gaussian, Inc.: Wallingford, CT, 2005.
(26) Moyano, A.; Pericàs, M. A.; Valent, A. *J. Org. Chem.* **1989**, *54*, 573.

JP8069817